ELSEVIER

Solid State Nuclear Magnetic Resonance 12 (1998) 211–220

SOLID STATE
Nuclear Magnetic
Resonance

The influence of adsorbed molecules on Na-sites in NaY zeolite investigated by triple-quantum ^{23}Na MAS NMR spectroscopy

Kan-Nian Hu, Lian-Pin Hwang *

Department of Chemistry, National Taiwan University, P.O. Box 23-34, Taipei, Taiwan
Institute of Atomic and Molecular Sciences, Academia Sinica, Taipei, Taiwan

Received 18 May 1998; accepted 3 July 1998

Abstract

The effect of hydration and benzene adsorption on ^{23}Na resonance and the quadrupolar interaction in NaY zeolites is studied by triple-quantum MAS ^{23}Na NMR spectroscopy. In the case of a C_6D_6/NaY system, the results show that with an increase in benzene loading, there is an up-field trend in isotropic chemical shift (δ_{CS}) and a decreasing second order quadrupolar effect (χ_s) for the site II sodium ions. It was found that adsorbed benzene molecules have a slight effect on the environment of sodium ions on site I. All the sodium sites in NaY are influenced upon hydration. The up-field shift of the sodium δ_{CS} reflects the effect of coordination of oxygen atoms on sodium cations due to hydration. The magnitude of χ_s for hydrated sodium sites increases and then falls off with water loading. The increase in χ_s is due to the initial hydration among SI-, SI′- and SII-sodium ions, while the decrease is the result of approaching the final stage of saturated hydration.

Keywords: Benzene adsorption in NaY; Hydrated NaY; MQMAS NMR; Isotropic chemical shift; Second order quadrupolar effect

1. Introduction

The catalytic properties of synthetic zeolites result from their capacity to adsorb a variety of molecular species into their connecting cages or/and channels within the framework structure where the adsorption sites are situated [1–3]. To understand the catalytic behavior of zeolites, one should first investigate not only the distribution of the cation sites in particular, but also the site interaction with the adsorbed molecules. Benzene is an essential probe in the study of the adsorption and enables description of aromatic site interaction in porous materials [4–6]. In NaY, the location for benzene has been studied using neutron diffraction [7,8], IR [9] and molecular dynamic calculation [10]. Two adsorption sites are revealed as the SII-Na and 12R window in the supercage. In addition, the presence of adsorbed water molecules in NaY causes not only a decrease in unit cell size but also an increase in the ionic mobility of sodium [11] and redistribution of sodium ion in zeolites [12].

The structure of zeolite Y, which is similar to that of the mineral faujasite, has been determined by X-ray diffraction [13,14], powder neutron diffraction

* Corresponding author. Department of Chemistry, National Taiwan University, P.O. Box 23-34, Taipei, Taiwan. Tel.: +886-2-23668287; Fax: +886-2-23620200; E-mail: nmra@po.iams.sinica.edu.tw

0926-2040/98/$19.00
PII: S0926-2040(98)00065-4

[15] and ^{29}Si NMR spectra [16]. Fig. 1 displays a portion of this structure with the correlated sites referred [17]. Each unit cell contains eight supercages, eight sodalite cages and 16 hexagonal prisms. The diameters of the 6-ring windows of the sodalite cages and the 12-ring windows of the supercages are about 2.4 Å and 7.4 Å, respectively. It is believed that water molecules may enter both the supercages and the sodalite cages, while benzene molecules may only be accommodated in the supercages.

In NaY zeolite, the properties of sodium cation sites are suitably investigated using solid-state NMR spectra because of their element-selectivity. Different solid-state NMR techniques including MAS, DOR and nutation have been used to determine the quadrupolar parameters of the crystallographically distinct sodium sites [18–20]. Recently, a multiple-quantum MAS NMR (MQMAS) proposed by Medek et al. [21] has been able to yield high resolution NMR spectra of half-integer quadrupolar nuclei such as ^{23}Na ($I = 3/2$), ^{27}Al ($I = 5/2$) and ^{17}O ($I = 5/2$) in inorganic salts, glasses and molecular sieves [22–29]. This technique can separate the overlapping signals and provides both the isotropic chemical shift (δ_{CS}) and the magnitude of the second order quadrupolar effect (χ_s). Its application to Na^+ in zeolite has yielded observed χ_s for the Na sites in the zeolites ranging from 1.0 to 3.1 MHz. These include SI-Na in NaY and NaEMT, sodium ions on 10-ring sites of NaZSM-5 and on 12-ring sites and sidepockets in NaMOR [26].

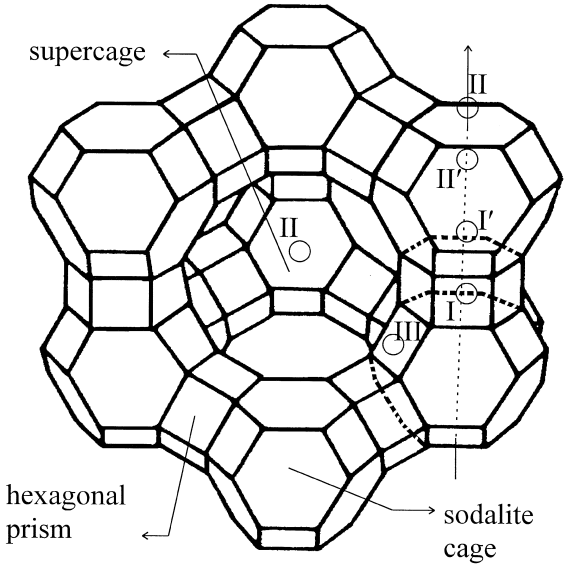

Fig. 1. Structure of faujasite, showing the structure of a supercage and the location of cation sites I–III. In NaY zeolite, only site I, I′ and II are referred to.

In this work, adsorption interaction and hydration effect in NaY with different benzene or water loading were studied by analyzing two parameters for ^{23}Na-isotropic chemical shift and the second order quadrupolar effect, as calculated using MQMAS NMR spectra. The correlated effects of benzene molecules on the sodium sites and ion mobility change due to hydration are discussed.

2. High-resolution MQMAS experiment

The MQMAS method combines MAS and two-dimensional experiment to average out the broadening due to the second order quadrupolar interaction of half-integer nuclear spin ($I > 1/2$). In the original two-pulse sequence [21], by correlating the evolution of the p-quantum coherence during t_1 and the observable single-quantum central transition coherence during t_2, an echo is observed at $t_2 = [pA_4(I,p)/A_4(I,1)]t_1$. Here the $A_4(I,p)$ is defined as [30]:

$$A_4(I,p) = 18I(I+1) - 34\left(\frac{p}{2}\right)^2 - 5 \qquad (1)$$

The method enables the refocus of anisotropy of the quadrupolar interaction. Since the center of mass of the anisotropic quadrupolar shift is zero, the first moment of resonance shift in the F2 dimension (or SQ axis) becomes:

$$\delta_2^{cm} = \delta_{CS} + A_0(I,1)B_0 \qquad (2)$$

where:

$$A_0(I,p) = I(I+1) - 3\left(\frac{p}{2}\right)^2 \qquad (3)$$

and:

$$B_0 = -\frac{3}{10\nu_0}\left(\frac{\chi_s}{2I(2I-1)}\right)^2 \qquad (4)$$

Here, ν_0 is the Larmor frequency in Hz. The second order quadrupolar effect is defined as $\chi_s \equiv$

$\chi(1+\eta^2/3)^{1/2}$ where the quadrupolar coupling constant $\chi \equiv e^2qQ/h$ in Hz and η is asymmetry parameter. The isotropic resonance shift in the F1 dimension (or 3Q axis) is obtained after a shearing transformation as mentioned previously [21]. It becomes:

$$\delta_1 = \frac{p(A_4(I,1) - A_4(I,p))}{A_4(I,1)}\delta_{CS} + \frac{p(A_0(I,p)A_4(I,1) - A_0(I,1)A_4(I,p))}{A_4(I,1)}B_0 \quad (5)$$

Using the above equations, δ_{CS} and χ_s can be solved.

3. Experimental

3.1. Sample preparation

The NaY (LZ-Y52, Si/Al = 2.4) used is supplied and characterized by STREM Chemicals, USA. C_6D_6 with a minimum purity of 99.5% was purchased from Merck, and no further purification process was used. For the studies of hydrated NaY zeolite, deionized water was used.

One small glass ball containing the required amount of adsorbate material was sealed and then admitted to the upper part of the sample tube with glass wool separating it from the NaY in the lower

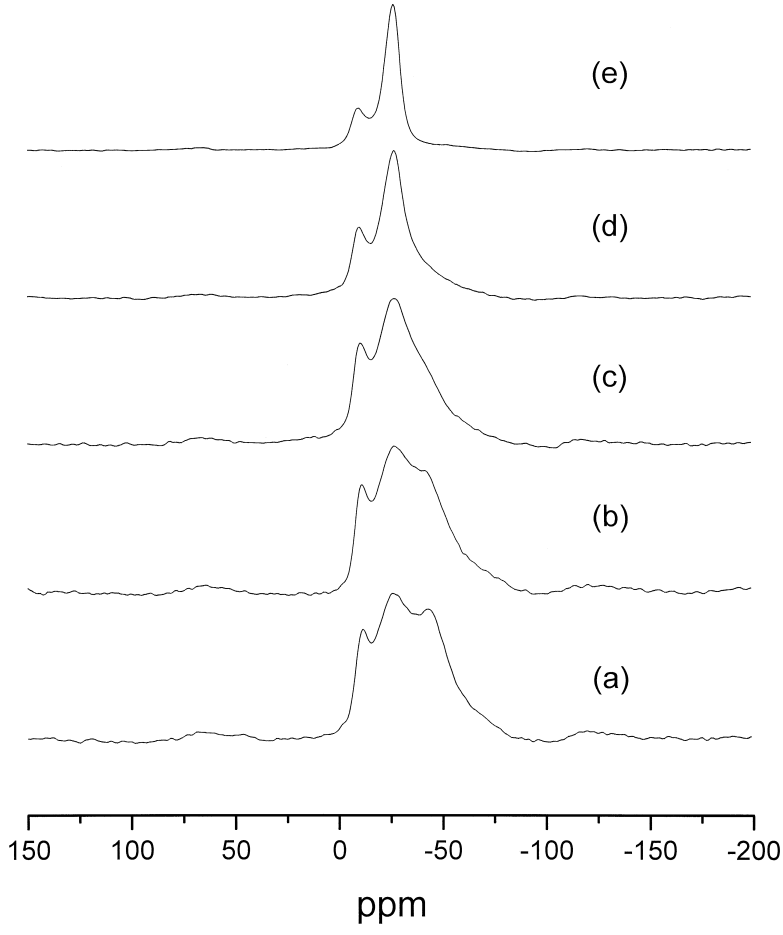

Fig. 2. ^{23}Na MAS NMR spectra of C_6D_6/NaY system including (a) $x = 0$, (b) $x = 0.3$, (c) $x = 0.8$, (d) $x = 2.0$, (e) $x = 5.0$ recorded at a resonance frequency of 132.3 MHz (11.75 T) with a spinning rate of 12 kHz. In the spectrum for dry NaY (a), the signal consists of a down field Gaussian peak as SI-Na and a second order quadrupole-splitting peak as SII-Na at high field.

part of the sample tube. The NaY was packed into a 4-mm ZrO_2 rotor which was then dehydrated under 10^{-5} Torr vacuum at 673 K for at least 12 h. After cooling, the tube was sealed with the dried NaY and C_6D_6-bearing ball inside. The adsorbate material ball was then broken by shaking the tube. Afterwards, the sample was kept at 353 K for 12 h to ensure a homogeneous distribution of adsorbate and finally the rotor was capped inside a dry box. Over a period of 4 months, the reproducibility of relaxation data was checked to ensure the stability and sealing of the sample. In the experiment on benzene effects, the sample was labeled as x C_6D_6/NaY which means x C_6D_6 molecules per supercage. Five NaY/benzene samples with $x = 0$, 0.3, 0.8, 2.0 and 5.0 were examined. The sample with $x = 5.0$ is considered to have saturated loading. To represent the loading of hydration, x H_2O/NaY means x H_2O molecules per unit cell. Four hydrated NaY samples with $x =$ 40, 88, 160 and 240 were examined.

3.2. NMR spectroscopy

The ^{23}Na MAS and MQMAS NMR measurements were carried out using a Bruker NMR spectrometer MSL-500 with a ^{23}Na resonance frequency of 132.3 MHz (11.75 T). The standard 4-mm Bruker MAS probe was used with a MAS frequency of ca. 12 kHz. To obtain the ^{23}Na MAS NMR spectra a single-pulse excitation of 0.65 μs corresponding to a $\pi/6$ flip angle and a repetition time of 800 ms were used. The 3QMAS NMR experiments were carried out using a three-pulse, z-filter sequence proposed by Amoureux et al. [31]. The triple quantum excitation pulse was 4.5 μs, and the conversion pulse was 2.6 μs. Both of these pulses were applied with the r.f. power set at 120 kHz. Observable magnetization was then induced after reducing the r.f. power to 12 kHz and applying a z-filter pulse of 16 μs which followed 5 μs after the second pulse. The t_1 was incremented by 8 μs. For each triple-quantum spectrum, 128 rows with 24 dummy scans and 1200 scans per row were recorded. The time-proportional-phase-increment (TPPI) was applied to the t_1 period of triple-quantum evolution in order to obtain a pure absorption spectrum. All ^{23}Na NMR shifts are referenced to the solid NaCl.

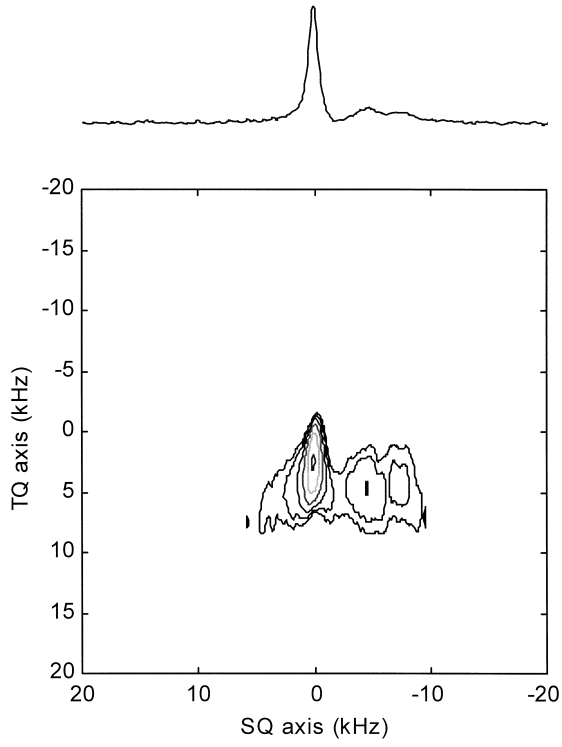

Fig. 3. 2D-contour plot of ^{23}Na 3QMAS NMR spectrum (topped with SQ-projections) for dry NaY recorded at a resonance frequency of 132.3 MHz (11.75 T) with a spinning rate of 12 kHz.

4. Results and discussion

For convenience of data processing, the contour plots of MQMAS NMR spectra are shown with respect to the individual resonance frequency. The calculated isotropic chemical shifts are later adjusted

Fig. 4. 2D-contour plots of ^{23}Na MAS NMR spectra (topped with SQ-projections) for C_6D_6/NaY system including (a) $x = 0.3$, (b) $x = 0.8$, (c) $x = 2.0$, (d) $x = 5.0$ recorded at a resonance frequency of 132.3 MHz (11.75 T) with a spinning rate of 12 kHz.

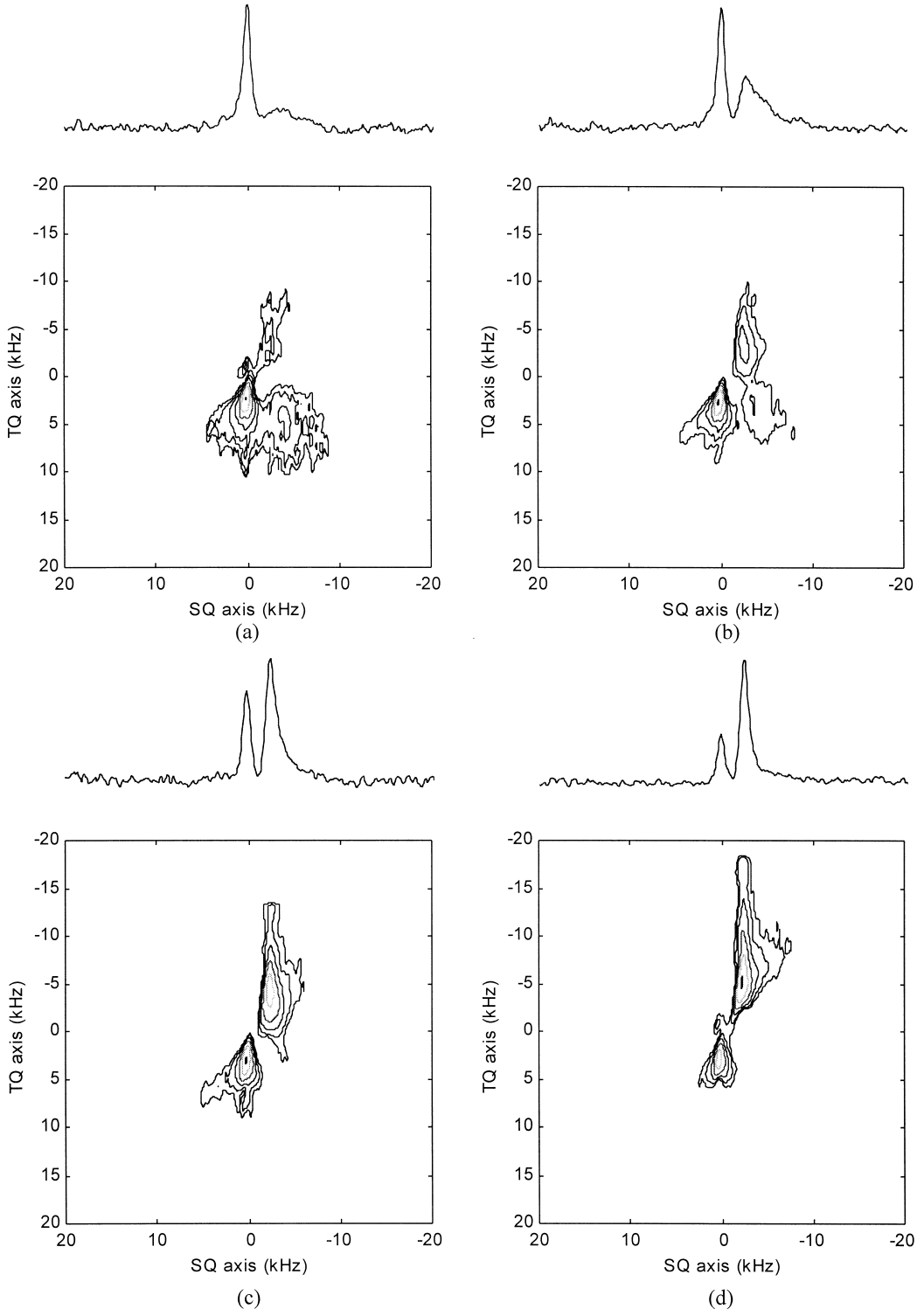
TQ axis (kHz)
SQ axis (kHz)
-20
-15
-10
-5
0
5
10
15
20
(a)
(b)
(c)
(d)

with respect to the signal for solid NaCl. The results are described below.

4.1. Effects of benzene adsorption

Fig. 2 shows the usual ^{23}Na-NMR spectra of various benzene-loaded NaY. With no loading of benzene, the Gaussian-like low field peak may be correlated to SI-Na and the high field peak with quadrupole-splitting to SII-Na [20]. With increasing benzene-loading the SII-Na signal changes dramatically from a quadrupole-splitting line shape to a Gaussian-like line shape. The quadrupolar coupling is apparently reduced. Furthermore, the benzene molecule attaching to the SII-Na may account for the reduction of the electric field gradient at Na. With decreasing loading, the signal for SII-Na shows two different environments at site II, i.e., the benzene molecules adsorb onto parts of the SII-Na. As benzene-loading gets higher, only the signal for benzene-adsorbed SII-Na is observed. Also, the SI′-Na signal was not detected and this is probably due to the relatively small concentration of this species.

In Fig. 3, the 2D-spectrum of dry NaY shows two groups of signals in which the higher frequency one along the SQ axis represents the SI-Na and the other is for the SII-Na. The SII-Na signal has a low S/N ratio due to the effect of a large quadrupolar interaction during the coherence transfers by nutation. The 2D-contour plot of dry NaY is the same as the result obtained by Hunger et al. [26]. In Fig. 4, the signal for adsorbed Na increases with the C_6D_6 loading as displayed in the 2D-contour plots of the samples with $x = 0.3$, 0.8, 2.0 and 5.0. On the other hand, the signal for bare SII-Na disappears for loading of over two molecules per supercage. Throughout the examination of all the 2D-spectra, we are still unable to identify the SI′-Na signal.

After analyzing the signal, as depicted in Table 1, small variations in the isotropic chemical shifts of SI-Na are observed among the samples and these reflect a small effect of down-field shift of SI-Na in the vicinity of adsorbed benzene molecules on SII or the 12R window site [8]. Within the experimental error the χ_s obtained for SI-Na is irrelevant to benzene loading. With increasing loading, the ring current effect of benzene may give rise to the decrease in the isotropic chemical shift of SII-Na adsorbed with benzene. Nevertheless, adsorption of benzene may reduce the electric field gradient at SII-Na as well, resulting in a decrease in magnitude of second order quadrupolar effect for SII-Na.

Table 1
The calculated parameters of isotropic chemical shifts (δ_{CS}) and second order quadrupolar effect (χ_s) of various benzene loaded NaY zeolites

C_6D_6/NaY	Na-sites	δ_{CS} (ppm)[a]	χ_s (MHz)[b]
$x = 0$	bare SI	−7.3	1.3
	bare SII	NA[c]	
$x = 0.3$	bare SI	−7.1	1.2
	bare SII	NA	
	C_6D_6-attached SII	NA[d]	
$x = 0.8$	bare SI	−6.5	1.2
	bare SII	NA	
	C_6D_6-attached SII	−21.9	2.3
$x = 2.0$	bare SI	−6.1	1.3
	bare SII	NA	
	C_6D_6-attached SII	−22.5	1.9
$x = 5.0$	bare SI	−6.1	1.2
	bare SII	NA	
	C_6D_6-attached SII	−23.3	1.7

[a] The calculated δ_{CS} is referenced to solid NaCl and has an error of ± 0.1 ppm.
[b] Error associated with χ_s is about ± 0.1 MHz.
[c] The signal of bare SII-Na cannot be resolved from MQMAS NMR spectrum, but its correlated parameter could be received from the curve fitting of the MAS NMR resonance line and revealed as $\delta_{CS} = -15$ ppm, $\chi = 3.9$ MHz, $\eta = 0$. As loading is above $x = 0.8$, the bare SII-Na is unseen on both MAS and MQMAS NMR spectra.
[d] The resolution is too low to be analyzed.

Previous neutron diffraction studies of the benzene/NaY system at 4 K and room temperature [7] have shown that some of the benzene attached to the SII-Na and the distance between SII-Na and the benzene molecule gets shorter with increasing benzene loading. As our results show, with increasing benzene loading, the upfield variation of isotropic chemical shift and the decreasing χ_s of SII-Na may be correlated with attachment of the benzene molecules to the SII-Na cations.

4.2. Effects of water adsorption

It is believed that water molecules are small enough to go through the 6-ring window on the face of the sodalite [32]. From the usual MAS- and

MQMAS-NMR spectra shown in Figs. 5 and 6, respectively, it can be seen that with the increasing H_2O loading the ^{23}Na signal changes from an overlapped line shape with a Gaussian peak and a quadrupolar splitting peak to a single Gaussian line. For the sample with a loading of $x = 40$, the broadening effect from the resonance of SII-Na can be clearly observed, while with loading above $x = 88$ only one merged Gaussian peak exists. The former observation reveals that the SII-Na is not significantly affected by low-loading hydration. Thus, one may infer that the adsorbed water molecules are preferentially situated in the sodalite cage. This is in good agreement with the conclusion obtained from a ^{129}Xe-NMR probing study of the hydrated NaY system [33]. Besides, it was found that when hydration is below 36 water molecules per unit cell, the xenon atom could not locate the presence of water molecules in the supercage.

In the MQMAS NMR spectrum for the $x = 40$ sample, Fig. 6a, the resolution of the broad shoulder peak at high field along the F2-axis is too low to be analyzed. However, the information inherent in the Gaussian-like signal is obtained in Table 2. The isotropic chemical shift for the Gaussian-like signal in hydrated NaY is found to shift to a higher field (-8.0 ppm) than that for SI-Na (-7.3 ppm) in dehydrated NaY. Moreover, the initially increasing values of χ_s reflect the degree of asymmetric coordination at sodium sites resulting from the hydration

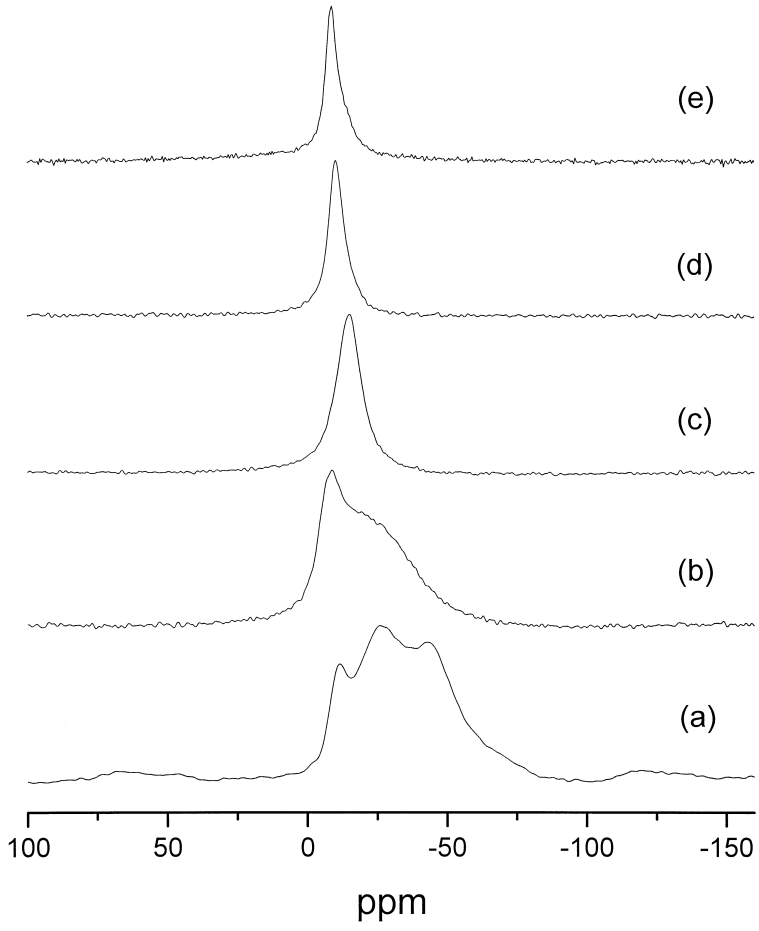

Fig. 5. ^{23}Na MAS NMR spectra of H_2O/NaY system including (a) $x = 0$, (b) $x = 40$, (c) $x = 88$, (d) $x = 160$, (e) $x = 240$ recorded at a resonance frequency of 132.3 MHz (11.75 T) with a spinning rate of 12 kHz.

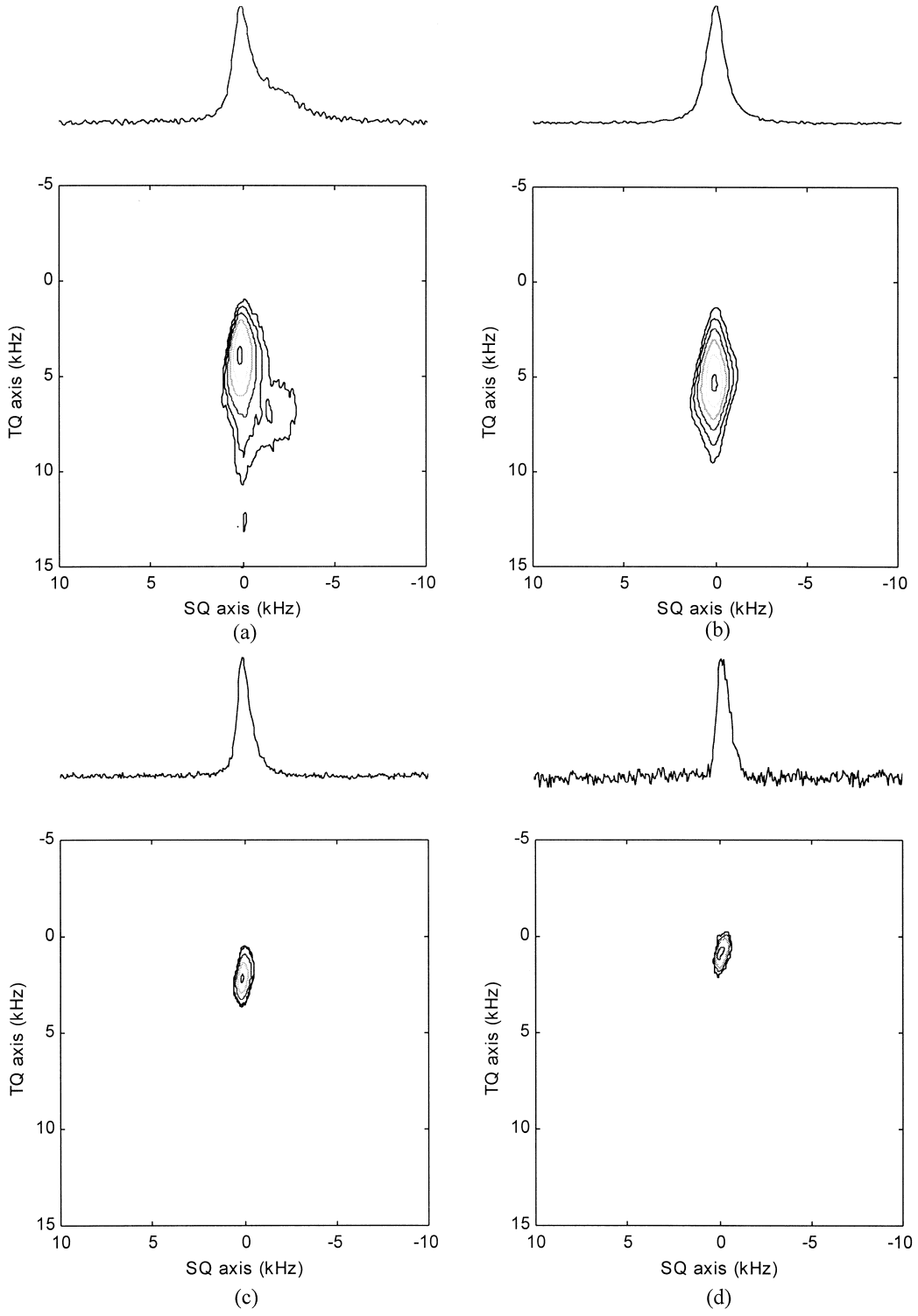
-5
0
5
10
15
TQ axis (kHz)
10
5
0
-5
-10
SQ axis (kHz)
(a)
(b)
(c)
(d)

Table 2
The calculated parameters of isotropic chemical shifts (δ_{CS}) and second order quadrupolar effect (χ_s) of NaY zeolites with various hydration

Hydrated NaY	Gaussian-like peak of ^{23}Na	δ_{CS} (ppm)[a]	χ_s (MHz)[b]
$x = 0$	dry SI	−7.3	1.3
$x = 40$	hydrated SI and SI′	−8.0	1.7
$x = 88$	hydrated SI, SI′ and SII[c]	−8.6	2.1
$x = 160$	hydrated SI, SI′ and SII	−8.7	1.3
$x = 240$	hydrated SI, SI′ and SII	−8.2	1.0

[a] The calculated δ_{CS} is referenced to solid NaCl and has an error of ±0.1 ppm.
[b] Error associated with χ_s is about ±0.1 MHz.
[c] When hydration is above $x = 40$, only single ^{23}Na resonance exists.

effect on the SII- and SI′-Na. Since SII- and SI′-Na are both situated on the 6-ring windows, the adsorbed water molecules may reduce the spatial differences between SII- and SI′-sodium and cause a similar chemical environment on both of them. When the hydrated NaY has a loading above $x = 88$, its χ_s falls off. It may reflect the symmetric arrangement of water molecules or/and the increase in the mobility of sodium ions and water molecules. Since the signal of triple-quantum is still observable, the mobility mentioned here involves only local motion which is confined within the neighborhood of the original sites. Furthermore, the same effect may be found also from a narrower line width in the MAS NMR spectra than that of $x = 40$, as shown in Fig. 5c–e. The results are consistent with the RAMAN experiments on the hydrated NaY by Ferwerda and van der Maas [11]. They concluded that in such a system, the presence of water increases the mobility of sodium cations and causes a broadening of the band for the O–T–O bending vibration. The other evidence of the increasing ion mobility can apparently result from the decrease in S/N ratio of the MQMAS NMR spectra for the samples with higher hydration.

For hydrated NaY samples, both δ_{CS} and χ_s differ from that of the SI-Na in dry NaY. Since the water molecules could hardly access the hexagonal prism cage (site I), the sodium cation there has to shift to the sodalite cage (site I′) in order to interact with the water molecules. The same phenomenon has been found in the XRD results for hydrated NaY [12]. In that experiment, an increased SI′-Na-occupancy is observed at low water loading. It means the coordination on SI′-Na cations is implemented by water molecules.

5. Conclusion

In this work, we apply two probe molecules, benzene and water, to study the adsorption effects on the sodium sites in NaY zeolites. In the case of benzene adsorption, only the SII-Na cations in the supercage, interacting directly with the adsorbed benzene molecules, were detected and this reflects the changes of isotropic chemical shift and second order quadrupolar effect. The SI-Na cations in the hexagonal prism cage show a slight change in isotropic chemical shift with increasing benzene loading. However, the quadrupolar interaction of SI-Na is almost unchanged and this indicates that the SI-Na environment is hardly affected by adsorbed benzene molecules in the supercages. It is well-known that benzene molecules are only allowed in the supercages and the results described above correlate well with this. Also, for fully hydrated NaY zeolite, all the sodium cations in it can interact with adsorbed water molecules. Since the adsorbed water molecules favor being situated in the sodalite cages, under low hydration (e.g., 40 H_2O per unit cell) the SII-Na can preserve its asymmetric environment and shows a broad NMR signal. Under higher water loading, the roll-off of the quadrupolar interaction of the hydrated sodium cations in NaY zeolites can be explained by the fact that the hydration reduces the electric field gradient at sodium sites resulting from the increase of mobility of those cations.

Chemical shift and quadrupolar interaction are indicative for the analysis of the interaction between the guest and host molecules. Thus, MQMAS is a feasible technique to obtain high resolution solid-state

Fig. 6. 2D-contour plots of ^{23}Na MAS NMR spectra (topped with SQ-projections) for H_2O/NaY system including (a) $x = 40$, (b) $x = 88$, (c) $x = 160$, (d) $x = 240$ recorded at a resonance frequency of 132.3 MHz (11.75 T) with a spinning rate of 12 kHz.

NMR spectra in which the parameters of isotropic chemical shift and second order quadrupolar effect are easily resolved.

Acknowledgements

We wish to thank the Chinese Petroleum for its financial support (Grant no. NSC 86-002) and K.N. Hu would like to thank the National Science Council of the Republic of China for the support of a graduate student fellowship (Grant no. NSC 87-2113-M-002-39).

References

[1] D.W. Breck, Zeolite Molecular Sieves: Structure, Chemistry and Use, Wiley, New York, 1974.
[2] J.A. Rabo (Ed.), Zeolite Chemistry and Catalysis, American Chemical Society, Washington, 1976.
[3] H. van Bekkum, E.M. Flanigen, J.C. Jansen (Eds.), Introduction to Zeolite Science and Practice, Elsevier, Amsterdam, 1991.
[4] A.K. Kiselev, V.I. Lygin, Infrared Spectra of Surface Compounds, Wiley, New York, 1975.
[5] B.L. Su, D. Barthomeuf, Zeolites 13 (1993) 623.
[6] A. de Mallmann, D. Barthomeuf, Zeolites 8 (1988) 292.
[7] A.N. Fitch, H. Jobic, A. Renouprez, J. Phys. Chem. 90 (1986) 1311.
[8] B.L. Su, J. Chem. Soc. Faraday Trans. 93 (1997) 1449.
[9] A.J. Renouprez, H. Jobic, R.C. Oberthur, Zeolites 5 (1985) 222.
[10] S.M. Auerbach, L.M. Bull, N.J. Henson, H.I. Metiu, A.K. Cheetham, J. Phys. Chem. 100 (1996) 5923.
[11] R. Ferwerda, J.H. van der Maas, Spectrochim. Acta, Part A 51 (1995) 2147.
[12] W.J. Mortier, E. van den Bossche, J.B. Uytterhoeven, Zeolites 4 (1984) 41.
[13] G.R. Eulenberger, D.P. Shoemaker, J.G. Keil, J. Phys. Chem. 71 (1967) 1812.
[14] D.H. Olsen, J. Phys. Chem. 72 (1968) 4366.
[15] A.K. Cheethan, M.M. Eddy, D.A. Jefferson, J.M. Thomas, Nature 299 (1982) 24.
[16] J. Klinowski, S. Ramdas, J.M. Thomas, G.A. Fyfe, J.S. Hartman, J. Chem. Soc. Faraday Trans. 2 (78) (1982) 1025.
[17] W.M. Meier, D.H. Olson, Atlas of Zeolite Structure Types, 2nd revised edn., Structure Commission of the International Zeolite Association, 1987.
[18] M. Hunger, G. Engelhardt, H. Koller, J. Weitkamp, Solid State Nucl. Magn. Reson. 2 (1993) 111.
[19] M. Feuerstein, M. Hunger, G. Engelhardt, J.P. Amoureux, Solid State Nucl. Magn. Reson. 7 (1996) 95.
[20] H. Koller, B. Burger, A.M. Schneider, G. Engelhardt, J. Weitkamp, Microporous Material 5 (1995) 219.
[21] A. Medek, J.S. Harwood, L. Frydman, J. Am. Chem. Soc. 117 (1995) 5317.
[22] C. Fernandez, J.P. Amoureux, Chem. Phys. Lett. 242 (1995) 449.
[23] P. Sarv, C. Fernandez, J.P. Amoureux, K. Keskinen, J. Phys. Chem. 100 (1996) 19223.
[24] J. Rocha, A.P. Esculcas, C. Fernandez, J.P. Amoureux, J. Phys. Chem. 100 (1996) 17889.
[25] C. Jäger, R. Hartmann, G. Kunath-Fandrei, O. Hirsch, P. Rehak, J. Vogel, M. Feike, H.W. Spiess, K. Herzog, B. Thomas, Ber. Bunsenges. Phys. Chem. 100 (1996) 1560.
[26] M. Hunger, P. Sarv, A. Samoson, Solid State Nucl. Magn. Reson. 9 (1997) 115.
[27] P. Sarv, B. Wichterlovà, J. Cejka, J. Phys. Chem. B 102 (1998) 1372.
[28] P.J. Dirken, S.C. Kohn, M.E. Smith, E.R.H. van Eck, Chem. Phys. Lett. 266 (1997) 568.
[29] J.P. Amoureux, F. Bauer, H. Ernst, C. Fernandez, D. Freude, D. Michel, U.T. Pingel, Chem. Phys. Lett. 285 (1998) 10.
[30] J.P. Amoureux, Solid State Nucl. Magn. Reson. 2 (1993) 83.
[31] J.P. Amoureux, C. Fernandez, S. Steuernagel, J. Magn. Reson. A 123 (1996) 116.
[32] R.M. Haniffa, K. Seff, J. Phys. Chem. B 102 (1998) 2688.
[33] A. Gedeon, T. Ito, J. Fraissard, Zeolite 8 (1988) 376.